Transient Cold Air Drainage down a Shallow Valley

L. MAHRT

NorthWest Research Associates, Redmond, Washington

JIELUN SUN, S. P. ONCLEY, AND T. W. HORST

National Center for Atmospheric Research, Boulder, Colorado*

(Manuscript received 16 January 2014, in final form 7 March 2014)

ABSTRACT

Drainage of cold air down a small valley and associated near-surface wind maxima are examined from 20 stations with sonic anemometers at 1 m and from a 20-m tower that includes six sonic anemometers in the lowest 5 m, deployed in the Shallow Cold Pool Experiment (SCP). The small valley is about 270 m wide and 12 m deep with a downvalley slope of 2%–3%. The momentum budget indicates that the flow is driven by the buoyancy deficit of the flow and opposed primarily by the stress divergence while the remaining terms are estimated to be at least an order of magnitude smaller. This analysis also reveals major difficulties in quantifying such a budget due to uncertainties in the measurements, sensitivity to choice of averaging time, and sensitivity to measurement heights.

Wind maxima occur as low as 0.5 m in the downvalley drainage flow—the lowest observational level. The downvalley cold air drainage and wind maxima are frequently disrupted by transient modes that sometimes lead to significant vertical mixing. On average, the downvalley drainage of cold air occurs with particularly weak turbulence with stronger turbulence above the drainage flow. The momentum flux profile responds to the shear reversal at the wind maximum on a vertical scale of 1 m or less, suggesting the important role of finescale turbulent diffusion.

1. Introduction

In the literature, most studies of drainage flows have concentrated on well-defined significant slopes with the goal of better physical understanding. Under clear skies with weak large-scale flow, even weak local slopes of a few percent or less can generate significant cold air drainage (Caughey and Palmer 1979; Blumen 1984; Aubinet et al. 2003). Cold air drainage leads to near-surface wind maxima, often in the lowest 10 m (Oerlemans et al. 1999; Grisogono and Oerlemans 2001; Mahrt et al. 2001; Oerlemans and Grisogono 2002; Parmhed et al. 2004; Haiden and Whiteman 2005; van der Avoird and Duynkerke 1999). Wind maxima in very thin drainage flows can even form well below 1 m, sometimes referred to as skin flows (Manins 1992; Mahrt et al. 2001; Nadeau et al. 2013). Frequently, the downvalley drainage is colder than the drainage down the side slopes, such that the side slope air flows over the top of the downvalley drainage. The colder air in the valley is then referred to as a cold pool (Whiteman 2000).

Haiden and Whiteman (2005) provide a comprehensive discussion of the budget equations and dynamics of flow over a sloped surface. In addition to such physics, drainage flows are often observed to be nonstationary on time scales of minutes to tens of minutes or longer (Doran and Horst 1981; Helmis 1996; Smeets et al. 1998; Monti et al. 2002). Even in simple valleys, the system of side slope and downvalley flows can be complex (Doran et al. 1990). Nonstationarity might be due to internal interactions between the turbulence, shear, and stratification as suggested by modeling studies (McNider 1982; Costa et al. 2011). Nonstationarity of drainage and downvalley flows have been related to the external influence of wavelike motions and other submesoscale modes (Mori and Kobayashi 1996; Amanatidis et al.

*The National Center for Atmospheric Research is sponsored by the National Science Foundation.

Corresponding author address: L. Mahrt, 2171 NW Kari Pl., Corvallis, OR 97330.
E-mail: mahrt@nwra.com

DOI: 10.1175/JAS-D-14-0010.1

1992; Papadopoulos et al. 1997; Monti et al. 2002; Sun et al. 2004; Mahrt 2010) or possibly the periodic exhaustion of the cold air supply. Stone and Hoard (1989) found oscillations of varying period but typically 5–10 min in a valley cold pool. Coulter and Martin (1991) found that drainage flows in tributary valleys were less developed when occurring with oscillatory modes. Poulos et al. (2007) showed that mountain waves and other gravity waves can modulate or eliminate drainage flows through an imposed pressure gradient. Slope flows are particularly vulnerable to external disturbances because they are more exposed compared to downvalley flow (Horst and Doran 1986). Nonetheless, Gryning et al. (1985) showed significant impact of gravity waves on a downvalley drainage flow. Porch et al. (1991) examined oscillations in a downvalley flow that were related to the influence of flow from a tributary valley. In addition to transient modes, Schmidli and Rotunno (2012) numerically demonstrated the potentially important and complex influence of regional winds and large-scale pressure gradients on the valley circulations.

Compared to studies in the literature, much of Earth's surface is characterized by weakly organized terrain. Little work has concentrated on drainage flow down common shallow valleys, which is the subject of this investigation. This study examines the nonstationarity of weak downvalley flows, particularly in terms of the near-surface wind maximum associated with such drainage flows. The study begins with a case study of the momentum budget of the downvalley flow (section 3) and then examines the vertical structure of the wind and turbulence within the downvalley flow (section 4). A simplified version of this analysis continues using all of the data in the field program (section 5). Although definite relationships emerge, the flow is sufficiently complex that this study must be considered as a preliminary investigation that identifies some basic interactions but leaves much unexplored.

2. Data

The Shallow Cold Pool Experiment (SCP) was conducted over semiarid grasslands in northeast Colorado at approximately 1660 m above sea level from 1 October to 1 December 2012 (https://www.eol.ucar.edu/field_projects/scp). The primary goal of the field program was to examine transient drainage flows and cold pools over common shallow topography. Figure 1 shows the domain and tower locations. The main valley is relatively small—roughly 12 m deep and 270 m across. The width of the valley bottom averages about 5 m with an average downvalley slope of 2%, increasing to about 3% at the upper end of the valley. This study analyzes primarily 1-m sonic anemometer data from a subset of the 20 stations and from the main tower at 0.5, 1, 2, 3, 4, 5, 10, and 20 m. To avoid bias in composited profiles, the tower data were eliminated for cases where one or more levels were missing. This study also analyzes a subset of the 1-Hz data from National Center for Atmospheric Research (NCAR) hygrothermometers deployed at the 0.5- and 2-m levels at the 20 stations. The temperature measurements from the hygrothermometers at 0.5 m are more accurate than the temperature measurements from the 1-m sonic anemometers and are used in this study. For estimation of the buoyancy term in the momentum budget, 1-m values of the temperature are computed by linearly interpolating between the temperatures at 0.5 and 2 m.

We analyze pressure data measured by the Vaisala PTB220B (Sun et al. 2013) at stations A3 and A8 and the Paroscientific Model 6000 in nano mode (8-kHz sampling) at the 1-m level on the main tower. The time dependence of the pressure gradient along the valley slope for the 3-h case study period (section 3) is estimated after removing the mean pressure for the case study period for each station. To some extent, removing the mean values of the pressure for each station reduces the impact of the synoptic pressure gradient, elevation differences, and offset errors. Removing the mean values of the pressure also removes the stationary part of the hydrostatic contribution from the horizontal temperature gradient associated with the cold pool. In this study, all heights will refer to the height above the local ground surface unless otherwise specified.

Turbulent fluctuations near the surface are nominally estimated as deviations from 5-min averages, which appear to include all of the turbulent scales even for the more windy weakly stable conditions. Such fluctuations are contaminated by nonturbulent motions for strongly stable conditions that lead to large scatter. For such conditions, the systematic flux is dominated by time scales less than 1 min—even less than 10 s for some of the records. The heat flux on scales larger than 5 min tends to be upward in the upper part of the tower layer for unknown reasons. We have decided against using a stability dependent averaging time, which complicates interpretation of the results. Use of 5-min averaging windows is a suitable overall compromise.

The analysis in section 5 is based on averaging quantities for different intervals of the wind speed, referred to as interval or bin averaging. Ratios are computed from averaged quantities rather than averaging the ratios directly. Averages are made only for those intervals with 10 or more samples.

Difficulties aligning sonic anemometers in complex terrain and examination of horizontal variations are discussed

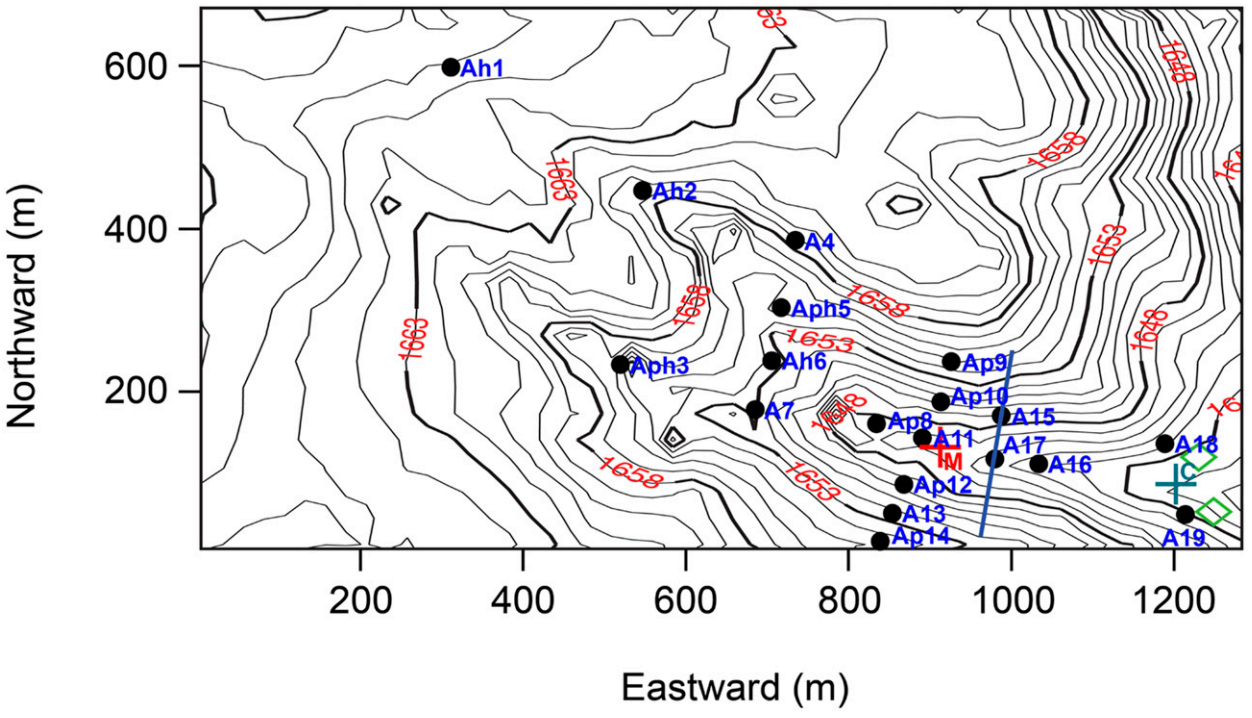

FIG. 1. A topographic (in m) map of the study area with sonic anemometer stations (black dots, the A stations) and the 20-m main tower (red M). The map also includes a short 3-m tower (green cross). Two sodars (green diamonds in the bottom-right corner) and a transect of fiberoptic temperature measurements (Thomas et al. 2012) indicated by the blue line are not used in this study. The h in the station labeling indicates inclusion of a 0.5-m two-dimensional Handar sonic anemometer while a p in the naming indicates inclusion of pressure measurements.

by Sun (2007). In this study, we computed fluxes only from the main tower. In a test calculation for the tower data, the coordinate system was rotated separately for 30° wind-direction sectors such that the mean vertical motion was zero for each sector for the entire dataset. The planar fit rotation was applied as a second approach. Rotation angles were 2° or less and the rotations did not lead to significant changes in the composited fluxes on the tower. A more comprehensive study is required. Here, unrotated data are used.

a. Stability

To classify stability in terms of a bulk Richardson number

$$\mathrm{Rb} \equiv \left(\frac{gz\Delta\theta}{\Theta}\right) \Big/ V^2 \qquad (1)$$

we choose $\Delta\theta$ as the difference of potential temperature between the 20- and 0.5-m levels on the tower. The wind speed V is computed from the 20-m level on the tower. Periods of near-neutral stratification, where the vertical temperature difference is too small to estimate, are eliminated by requiring that $\mathrm{Rb} > 0.01$ and $\Delta\theta > 0.01$ K.

The flow cannot be rigorously classified in terms of a single parameter, such as Rb, because advection, nonstationarity, curvature of the wind profile, structure of the flow above the tower layer, surface roughness, and heterogeneity can all be important influences. The current study uses the bulk Richardson number or the wind speed at 20 m to nominally classify the flow into different classes.

b. Representation of the turbulence

The strength of the turbulence is generally represented in terms of the turbulent kinetic energy. With strongly stable conditions, the horizontal velocity components can be dominated by primarily horizontal motions with very little correlation with the corresponding extremely weak vertical motions. In this respect, the horizontal velocity fluctuations are due mainly to nonturbulent modes. As a result, the standard deviation of the vertical velocity fluctuations σ_w is a better indicator of the turbulence than the kinetic energy. However, with sufficiently strong stratification, the linear correlation coefficient between vertical velocity fluctuations and fluctuations of horizontal wind components and temperature decrease below 0.1 (Mahrt 2011) owing to increasing importance of nonturbulent motions (often wavelike) to the fluctuating vertical motion. As a possible result, σ_w retains significant values when the wind speed and/or shear become extremely small. Even

attempts to carefully adjust the averaging time to filter out nonturbulent motions can fail because turbulent and nonturbulent fluctuations appear to overlap in scale, as suggested by the small correlations between vertical velocity and temperature fluctuations even for time scales less than 10.

Mahrt et al. (2013) instead used

$$V_{w\theta} \equiv -\frac{\overline{w'\theta'}}{\sigma_\theta} = -R_{w\theta}\sigma_w, \qquad (2)$$

where $R_{w\theta}$ is the correlation between the potential temperature and vertical velocity fluctuations. This velocity scale more accurately represents the turbulence responsible for the mixing and approaches values much smaller than those for σ_w with vanishing wind speed or wind shear, as is examined in a separate study. We have based our velocity scale on the heat flux rather than on the momentum flux because heat flux is less erratic than the momentum flux for very stable conditions. Even then, $V_{w\theta}$ based on 5-min averages can show large scatter. The quantity $V_{w\theta}$ is most useful after compositing to reduce the large variability, as is done here.

c. *Quantification of wind maxima*

Identifying wind maxima requires specification of the decrease of wind speed above the maxima. Wind maxima are sought where the speed of the 5-min-averaged wind vector decreases above the wind maxima by a certain total amount (δV) or by a certain rate ($\partial V/\partial z$) where V is the wind speed. Some of the profiles at the main tower include multiple wind maxima separated by wind minima. The instrument configuration presumably fails to resolve some wind maxima.

This study focuses on near-surface wind maxima mainly in the lowest 5 m, which is measured with sonic anemometers at 0.5, 1, 2, 3, 4, and 5 m on the main tower. The 2-m level is the closest level to the surface for detecting wind maxima with adequate information on vertical structure below the wind maxima. Our study examines the wind maxima at this level in some detail and then includes wind maxima at other levels for comparison. We employ a crude selection method where the wind speed at 2 m must exceed the 5-m wind speed by a threshold value. The threshold values are specified to be 0.3 m s^{-1} (strong criteria) and 0.1 m s^{-1} (weak criteria), corresponding to a shear magnitude of 0.1 and 0.03 s^{-1}, respectively. Although the threshold value may appear to be small, many of the near-surface wind maxima occur with speeds less than 1 m s^{-1}. The stronger criteria limit the analysis to the better defined wind maxima while the weaker selection criteria provide a larger sample.

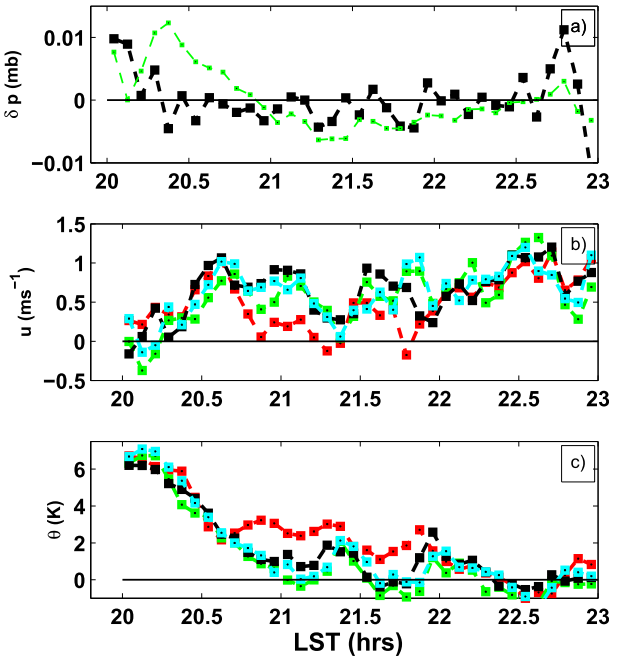

FIG. 2. (a) The surface pressure (mb) at A8 minus that at A3 (black), and the pressure at the main tower minus that at A8 (green) for the case study period. (b) The downvalley wind speed (m s^{-1}) for A3 (red), A7 (black), A8 (green), and A11 (cyan). (c) The 0.5-m potential temperature (K) at A3 (red), A7 (black), A8 (green), and A11 (cyan).

Manually selecting wind maxima produces a different set of maxima although most of the selected wind maxima occur in both sets. Manual methods require subjective judgment. Other automated methods were applied, such as specifying a minimum decrease of wind speed from the maxima to the next overlying observation level or to an automated detected wind minimum. The qualitative conclusions of this study are not affected by the choice of the detection method.

3. The downvalley momentum budget

Airflow down the valley can be identified as cold air drainage if it is driven primarily by buoyancy. Evaluation of the momentum budget is complex and subject to significant errors. The budget cannot be left to automated procedures and requires a case study approach. We construct a case study analysis of the momentum budget for the early part of the night beginning on day of year (DOY) 322 (evening of 17 November 2012). This period is characteristic of typical cold air drainage down the valley in SCP. Formation of the cold air in the valley develops quickly after dissipation of the cloud cover and near simultaneous decrease of the regional–synoptic flow at about 2000 local standard time (LST), which in turn leads to substantial cooling near the surface (Fig. 2c). This

downvalley drainage flow is eliminated as a dominant feature around 2300 LST when the regional northerly flow increases. This determines the end of the case study period. The downvalley drainage flow reforms intermittently throughout the remainder of the night as is typical for this field program.

The SCP valley includes some three-dimensional structure including tributary gullies, channeling, and variation of valley width and height of the side slopes. Here we pursue simplified equations of motion where we have assumed two-dimensional downvalley flow in a coordinate system rotated to be parallel to a constant slope. After removal of a hydrostatic basic state, the equation of motion for the downslope flow (Mahrt 1982; Haiden and Whiteman 2005) becomes

$$\frac{d\overline{u}}{dt} = -g\frac{\theta^*}{\theta_{oo}}\sin(\gamma) + \frac{g}{\theta_{oo}}\frac{\partial([\theta^*]h)}{\partial x}\cos(\gamma) - \alpha_{oo}\frac{\partial(p_n^*)}{\partial x} - \alpha_{oo}\frac{\partial p_{oo}}{\partial X}\cos(\gamma) - \frac{\partial\overline{w'u'}}{\partial z}, \quad (3)$$

where the x coordinate is directed eastward down the slope of magnitude of γ, z is the coordinate perpendicular to the surface, and X is directed horizontally in the eastward direction in the unrotated coordinate system. The terms on the right-hand side are the buoyancy term, thermal wind term, nonhydrostatic pressure gradient term, large-scale pressure gradient, and the momentum flux divergence term. The brackets $[\cdot]$ refer to a vertical average over the flow of depth h and the asterisks indicate deviations of the time-averaged flow from a hydrostatic basic state flow (α_{oo}, θ_{oo}, p_{oo}) at a fixed point; α is the specific volume and p_n^* is the nonhydrostatic component of the pressure.

In practice, the basic state flow can be defined as a horizontal average in which case θ^* and p^* are the deviation of the local time average (here 5 min) on the sloped surface from a horizontal average at a constant elevation in absolute space (perpendicular to gravity). The spatially averaged potential temperature is inferred as the potential temperature at the same absolute level on the tower in the valley. That is, the temperature on the tower above the downvalley drainage flow is assumed to be representative of an area average on the scale of the valley although the inferred area of the average is not actually known. Estimation of the buoyancy term is always problematic in studies of cold air drainage and makes examination of the momentum budget somewhat qualitative.

The overbar in the last term indicates the local time average (here 5 min) for estimating the momentum flux in the downvalley direction and primes indicate deviations from this average. The term $\partial p_{oo}/\partial X$ is the pressure gradient associated with regional and larger scales winds and is presumably approximately height independent over the thin drainage flow. The large-scale horizontal pressure gradient, $\partial p_{oo}/\partial X$, is largely eliminated from the ''observed'' along-slope pressure gradient by the removal of the 3-h time-averaged pressure for each station. The Coriolis term for the current flow is less than 10^{-4} m s^{-2} and is an order of magnitude smaller than the important terms in Eq. (3). Therefore, it has been neglected. The acceleration term on the left-hand side includes any advection by the larger-scale flow.

Quantitative evaluation of Eq. (3) is problematic even with the dense SCP network. Nonetheless, insights on the development of the downvalley flow is afforded by examining the spatial and temporal evolution of the wind and temperature field during the 3-h period (2000–2300 LST) in the framework of Eq. (3). The analysis of the terms in Eq. (3) focuses on the upper end of the main valley at A7 (Fig. 1). One can view the upstream southern gully as an extension of the main valley in that it follows the same west-northwest axis. In addition, the southern gully is the main source of air for the main valley during the case study period while the brief flow down the northern gully is eliminated by the onset of ambient north-northeast flow after 2030 LST.

The buoyancy term, baroclinic (thermal wind) term, and pressure gradient term are easier to evaluate at A7 (Fig. 1) than at stations farther down the valley. However, the analysis at A7 uses the stress divergence from the main tower, which is of uncertain applicability to the stress divergence at A7. The buoyancy term is difficult to estimate at the main tower because of inadequate estimation of the area-averaged temperature with reference to a near-surface level on the tower. Also, it is not possible to evaluate the horizontal pressure gradient centered at the main tower owing to lack of suitable pressure measurements downvalley from the tower.

a. Buoyancy term

The observed generation of downvalley flow is presumably due to the buoyancy term. If the surface potential temperature at a given point on the slope is less than the horizontal average of the potential temperature such that $\theta^* < 0$, then the buoyancy term acts to accelerate the flow down the slope. The buoyancy θ^* of the surface flow on the side slopes and in the tributary gullies is generally negative based on the 0.5-m potential temperature. The buoyancy deficit at station A7 develops during the rapid cooling period beginning around 2000 LST and reaches about 4 K by 2030 LST (Fig. 3). The buoyancy deficit at the up gully station A3 is about the same as that at station A7 although short term differences are substantial in spite of the small separation distance of

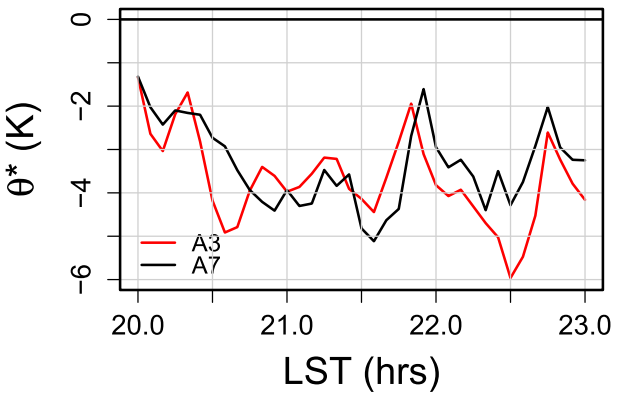

FIG. 3. The buoyancy θ^* for the case study period based on the 0.5-m temperature for the southern tributary gully station A3 (red) and the station at the mouth of the southern tributary gully A7 (black).

only 150 m. Even during the period of relatively persistent downvalley flow, the buoyancy term at a given point exhibits considerable short term variability.

The downvalley slope at A7 is 3%. The buoyancy deficit averages about 3 K between 2030 and 2230. The corresponding order of magnitude of the buoyancy term is estimated to be $3 \times 10^{-3}\,\mathrm{m\,s^{-2}}$. Similar results are obtained for station A3.

b. Baroclinic term (thermal wind)

The second term on the right-hand side of Eq. (3) is the baroclinic term where $[\theta^*]$ is the vertical average of the potential temperature over the thin depth of the cold air drainage. The along-slope pressure gradient due to the thermal wind acts to decelerate the drainage flow (adverse pressure gradient) in the upper part of the valley where the temperature decreases in the downvalley direction.

The depth of the drainage flow h and the strongest stratification in the valley at the main tower both reach about 5 m (section 4). This depth may be smaller in the upper part of the valley. We estimate the along-valley temperature gradient at station 7 in terms of the potential temperatures at A3 and A8, which provides a centered difference estimate for A7 (Fig. 1). The temperature measurements at the A stations indicate that the along-slope temperature gradient decreases with height and becomes significantly smaller at 2 m compared to 0.5 m. Viewing h as a local scaling depth for the time-averaged cold air drainage at A7, we assign it to be 2 m.

The along-slope temperature gradient between stations A3 and A8 over the 300-m separation distance is quite weak prior to 2030 LST and becomes about 1 K after 2030 LST. The baroclinic term due to along-slope temperature variations within the drainage flow is then estimated to be about $2 \times 10^{-4}\,\mathrm{m\,s^{-2}}$. This value is about an order of magnitude smaller than the buoyancy term. Horst and Doran (1986), Papadopoulos et al. (1997), and Mahrt et al. (1982) also found this term to be unimportant, at least for relatively thin drainage flows.

c. Measured pressure gradient

The measured along-valley pressure gradient term includes contributions from the baroclinic pressure gradient [second term on the right-hand side of Eq. (3)], the nonhydrostatic pressure gradient term (third term), and the pressure gradient above the drainage flow (fourth term). Recall that the pressure p^* is theoretically the deviation from a hydrostatic basic state. In practice, the stationary part of the baroclinic term has also been eliminated by removing the 3-h mean values from the observed pressure (section 2). The along-valley pressure difference is computed between two pairs of stations, A8 and A3 (within the southern gully), and between A8 and the main tower in the main valley (Fig. 1).

At 2000 LST, the pressure difference in the x direction, $p(\mathrm{A8}) - p(\mathrm{A3})$, is positive (higher relative pressure to the east), which opposes the downvalley flow (Fig. 2a). At this time, the pressure gradient term between stations A3 and A8 is estimated to be about $10^{-4}\,\mathrm{m\,s^{-2}}$, which is about an order of magnitude smaller than the buoyancy term. The measured pressure gradient term then decreases with time to very small values by 2030 LST and remains very weak throughout the rest of the case study period.

d. Stress divergence term

The stress divergence term cannot be directly evaluated at the A stations because they have a sonic anemometer only at one level. At the main tower during the period of strongly stratified downvalley cold air drainage (2030–2230 LST), the momentum flux $\overline{w'u'}$ is upward above the wind maximum at approximately 0.5–1 m (Fig. 4). This upward flux is associated with upward transport of westerly downvalley flow and downward transport of easterly upvalley flow. The stress approximately vanishes at the level of the wind maximum (Fig. 4) where the shear is small. The momentum flux is weak downward at the 0.5-m level associated with increasing westerly speed with height below the wind maximum. The momentum flux at the 0.5-m level may be underestimated as a result of sonic anemometer pathlength averaging (Horst and Oncley 2006) and consequential omission of transport by the turbulence on the scale of the sonic anemometer pathlength and smaller. During shorter periods of 5 or 10 min when the wind maximum is temporarily higher than 1 m, more significant downward momentum flux is observed below the wind maximum (not shown).

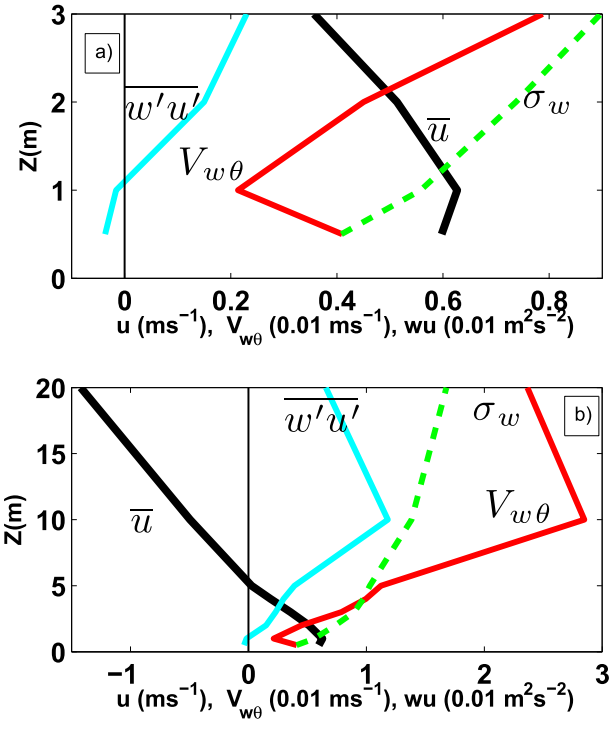

FIG. 4. Vertical profiles of the along-valley flow (m s^{-1}, black), along-valley momentum flux (0.01 m^2 s^{-2}, cyan), σ_w (0.1 m s^{-1}, green dashed), $V_{w\theta}$ (0.01 m s^{-1}, red), all averaged over 2030–2230 LST for (a) the lowest 3 m and (b) the entire 20-m tower layer.

The positive $\overline{w'u'}$ increases with height up to the 10-m level (Fig. 4b) where the shear is still significant and the stratification is much weaker than in the surface-based strong stratification below 5 m. The quantity $\overline{w'u'}$ decreases above 10 m in what might be the lower part of the regional boundary layer that advects over the shallow valley. The stress divergence term between the surface and 10 m is about 1.3×10^{-3} m s^{-2} at the main tower and acts as an important sink of downvalley momentum. Because the vertical stress profile is roughly linear, the stress divergence in the lowest 5 m has a similar value.

e. Acceleration term

The imbalance between the terms on the right-hand side of Eq. (3) leads to net acceleration. The Lagrangian acceleration ($d\overline{u}/dt$) between stations A3 and A7 is estimated based on the downvalley velocities averaged over both stations between 2030 and 2230 LST, equal to about 0.5 m s^{-1}. A Lagrangian parcel traveling with this speed requires 300 s to travel the 150 m between A3 and A7. The increase of the downvalley speed between A3 and A7 is 0.27 m s^{-1}. This increase of speed over the 5-min travel time corresponds to an acceleration of approximately 10^{-3} m s^{-2}. This is the same order of magnitude of the acceleration as the above force imbalance for Eq. (3). Local accelerations associated with the transient nonstationary modes are larger over short periods but do not lead to significant net acceleration when averaged over the 2-h period.

4. Vertical structure

We now examine the vertical structure of the flow during the case study period. Noting that the wind speed vanishes at the surface, the wind maximum for the downwind velocity profile averaged over 2030–2230 LST occurs at about 1 m (Fig. 4), which is about 0.2 of the depth of the strongest part of the inversion. This is on the lower end of the range found by Horst and Doran (1986), though their estimates were constructed from observations on side slopes rather than downvalley drainage flows within the cold pool where the inversion is more protected.

The composited σ_w increases with height across the 20-m tower layer (Fig. 4b). In contrast, the composited $V_{w\theta}$, which is expected to better represent the turbulence responsible for the mixing, decreases from 0.5 to 1 m where it reaches a minimum (Fig. 4a). Because the shear is almost independent of height above the wind maximum and the stratification decreases rapidly with height above the wind maximum, the gradient Richardson number (not shown) decreases with height. As an apparent result, the stress and the turbulence represented by $V_{w\theta}$ both increase with height above the wind maximum up to 10 m. Between 10 and 20 m, the stress and $V_{w\theta}$ both decrease with height while σ_w increases with height.

The wind speed at 1 m (Fig. 5a) and the wind profile (Fig. 5b) vary considerably during the period of downvalley cold air drainage (2030–2230 LST). The wind profile is much more variable than the temperature profile (not shown). Within the case study period, the relationships between the wind maximum, temperature, and turbulence are weak probably because of nonequilibrium turbulence associated with the nonstationarity. In general, the downvalley flow at the surface is weaker when the easterly flow at the top of the tower is stronger, probably because of increased downward mixing of easterly momentum.

The near-surface wind maxima around 1 m and the corresponding apparent height reversal of the momentum flux across the wind maximum imply that compliance with surface-layer similarity theory would be confined to a depth that is small compared to 1 m. However, such low levels are not high compared to the depth of the roughness elements (tens of centimeters) such that surface-layer similarity theory is not formally valid at any level. There is no surface layer that is well

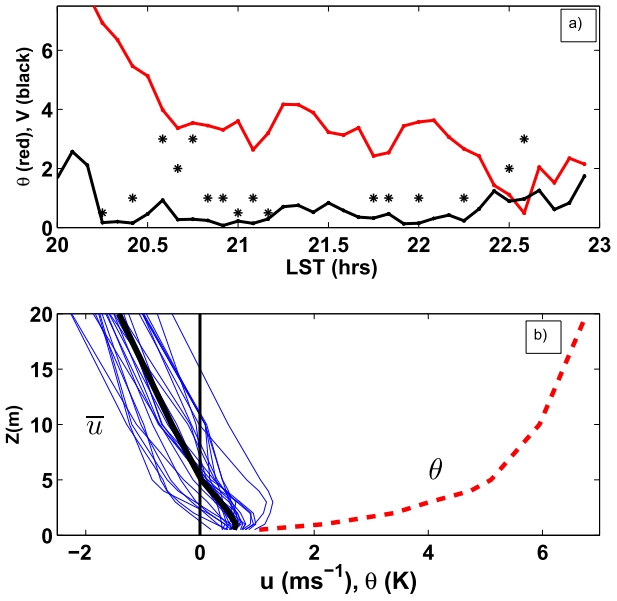

FIG. 5. (a) Height of the maximum wind speed in the lowest 5 m (black asterisks) based on the weak selection criteria (section 2) for the case study period, the 1-m wind speed (black), and the temperature at 2 m less the minimum value for the 2-h period (red). (b) Profiles for the period from 2030 to 2230 LST (when the vertical structure is most stationary) for the individual 5-min-averaged downvalley flow (blue lines), the average over the 2-h period for the downvalley flow (black), and the potential temperature (red dashed).

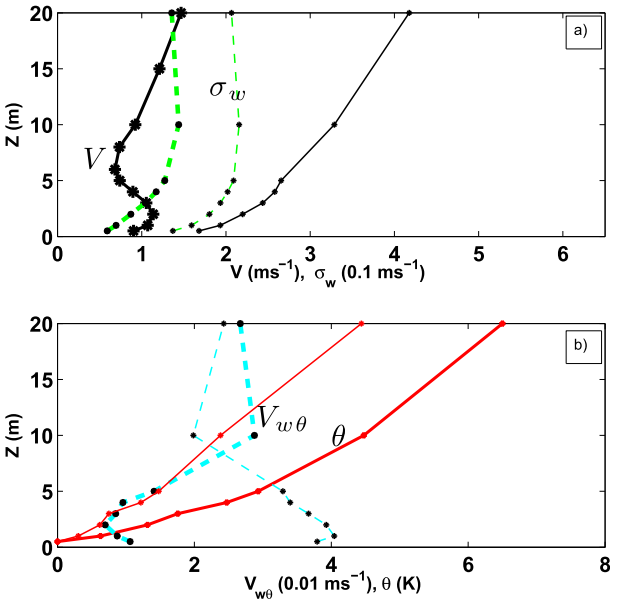

FIG. 6. Profiles composited for all of the 5-min periods during the field program (thin lines) and all of the periods with a wind speed maximum at 2 m (thick lines) for (a) the wind speed (m s^{-1}, black) and σ_w (0.1 m s^{-1}, green) and (b) θ (K, red) and $V_{w\theta}$ (0.01 m s^{-1}, cyan). Potential temperature is relative to the surface value.

below the wind maxima but above the roughness sublayer. The drag coefficient and transfer coefficient for heat are sensitive to choice of height in a way not described by similarity theory. As one example, these coefficients evaluated at 5 m would be very large because the speed is quite small near the reversal from downvalley to upvalley flow.

5. "Climatology" of wind maxima during the field program

The evaluation of the momentum budget, even qualitatively, could not be routinely carried out for the entire field program and necessitated the above case study. Even the detection of the downvalley cold air drainage cannot be left to automated procedures because it occurs with a variety of structures. However, the formation of near-surface wind maxima in the downvalley drainage flow indicates local generation of cold air drainage in contrast to larger-scale flow in the downvalley direction where the buoyancy force is not significant. Thus, near-surface wind maxima are a good indicator of drainage of cold air down the valley.

Here, we examine the behavior of the flow structure over the entire field program between the hours of 1900 and 0600. In general, near-surface wind maxima are much less frequent when the regional wind speed measured at 20 m exceeds a few meters per second or when the bulk Richardson number is small compared to unity. The very stable class (Rb $>$ 1) includes 21% of the 5-min records. The field program was dominated by relatively windy conditions or by conditions of some cloud cover.

Near-surface wind maxima (below 5 m) occur for 12% of the very stable 5-min records for the strict criteria (section 2) and for 34% of the records for the less strict condition. Presumably, some wind maxima fail to be resolved by the vertical resolution of the observations. Some subjectively identified wind maxima are missed by the automated selection procedure (section 2). Although numerous wind maxima also occur at or above 5 m, the current study focuses on those wind maxima occurring below 5 m, which are almost always downvalley drainage of cold air. Roughly half of the wind speed maxima below 5 m with the stricter criteria occur as a single isolated 5-min period, and no wind maxima at a given height survive longer than 35 min. At the same time, near-surface wind maxima may occur intermittently over periods of several hours or more. Averaging profiles over such periods generally produces a well-defined wind maximum.

As an example of the vertical structure in the presence of near-surface wind maxima, we examine the composited vertical structure for all 5-min periods with wind maxima detected at 2 m using the strict threshold criteria (thick lines, Fig. 6) and compared with the composite

over cases without such wind maxima (thin lines, Fig. 6). Although most of the wind maxima occur below 2 m, the 2-m level provides two levels of sonic anemometers below the wind maxima (0.5 and 1.0 m). With the strict criteria for the wind maximum, 49 five-minute periods are detected with the wind maximum at 2 m. Because the wind maxima tend to occur with stronger stability and weaker regional flow, the averaged wind speed with wind maxima (thick black, Fig. 6a) is roughly half of the composited wind speed for all of the cases (thin lines). The stratification in the lowest 5 m (red lines, Fig. 6b) is almost twice as large for the class with wind maxima in the lowest 5 m as compared to that for all of the data.

The composited σ_w increases with height (Fig. 6a), with (thick dashed green line) or without (thin dashed green line) wind maxima at 2 m. Increase of σ_w within and above drainage flows has been observed by Coulter and Martin (1996) and others. In contrast, $V_{w\theta}$ sharply distinguishes between the cases with and without wind maxima at 2 m (cyan lines, Fig. 6b). For the overall class, $V_{w\theta}$ decreases linearly with height up to 10 m. The quantity $V_{w\theta}$ for the class with wind maxima at 2 m decreases with height and reaches a minimum at 2 m, possibly because of nearly vanishing shear at the level of the wind maximum (some directional shear remains). Such a minimum suggests that the turbulence above the wind maxima is partially decoupled from the surface turbulence (Horst and Doran 1988; Grisogono et al. 2007; Conangla and Cuxart 2006).

The composited $V_{w\theta}$ increases by more than a factor of three above the wind maximum where $V_{w\theta}$ is as strong as for the windier class with no wind maxima at 2 m (Fig. 6b). The shear on the upper side of the wind maximum is significant and roughly independent of height up to 5 m while the stratification decreases with height. It is not known if the inflection point above the wind maximum leads to instability and generation of turbulence. In addition, the wind direction often rotates from downvalley flow near the surface to more cross valley in upper part of the tower layer, possibly enhancing the generation of turbulence through directional shear. In either case, the downvalley cold air drainage and associated wind maxima occur in a rather thin layer of very weak turbulence with more significant turbulence above. The downvalley drainage flow and wind maximum survive in very weak turbulence and are eliminated when more significant turbulence develops near the surface. Results are similar for selection of wind maxima at other levels within the lowest 5 m although the observed impact of the wind maxima on the turbulence decreases with the height of the wind maximum.

For additional perspective, we now consider only very stable cases (Rb $>$ 1, Fig. 7) with wind maxima at 2 m

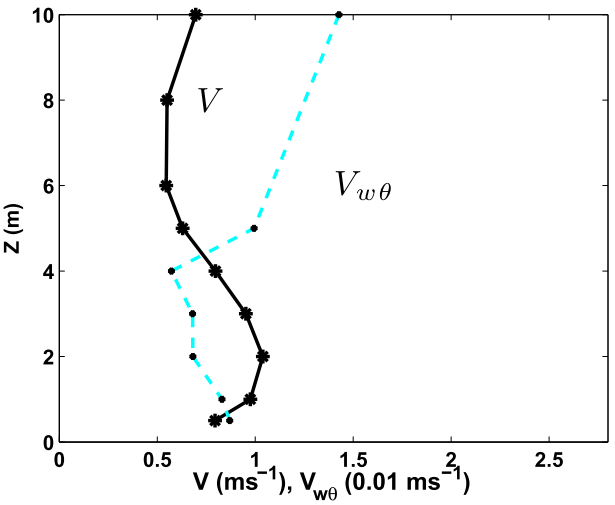

FIG. 7. Profiles composited over all of the very stable (Rb $>$ 1) 5-min periods during the field program with a speed maximum at 2 m for the wind speed (m s^{-1}, black) and $V_{w\theta}$ (0.01 m s^{-1}, cyan).

with the strict criteria for detection of wind maxima. The condition on Rb eliminates 10 five-minute periods, leaving 39 periods where the wind maximum is at 2 m. As before, the turbulence based on $V_{w\theta}$ decreases with height within the drainage flow, reaches a local minimum at the wind maximum, and increases significantly in the weaker stratification above the drainage flow.

The increase of turbulence with height above the downvalley cold air drainage for strong stability corresponds to a sloped-terrain version of the top down very stable boundary layer defined by Williams et al. (2013). The periods between the downvalley cold air drainage often appear to be most like the near-neutral shallow stable boundary layer defined by Williams et al. (2013) where the bulk Richardson number [Eq. (1)] falls below 0.03.

For relatively clear skies with significant radiative cooling at the surface ($R_{net} < -50$ W m^{-2}), the percentage of the time occupied by wind maxima below 5 m decreases almost linearly with increasing speed of the westerly component at 20 m (black line, Fig. 8a). Stronger winds leads to more vertical mixing and elimination of the wind maximum. However, the percentage of the time occupied by wind maxima below 5 m varies less systematically with increasing cross-valley flow although the overall trend is comparable (cyan, Fig. 8).

6. Conclusions

Cold air drainage down a shallow valley with a 2%–3% slope is examined with data from a 20-m tower and an extensive network of sonic anemometers that includes slow response pressure and temperature sensors. Although the terrain relief is of smaller amplitude compared to

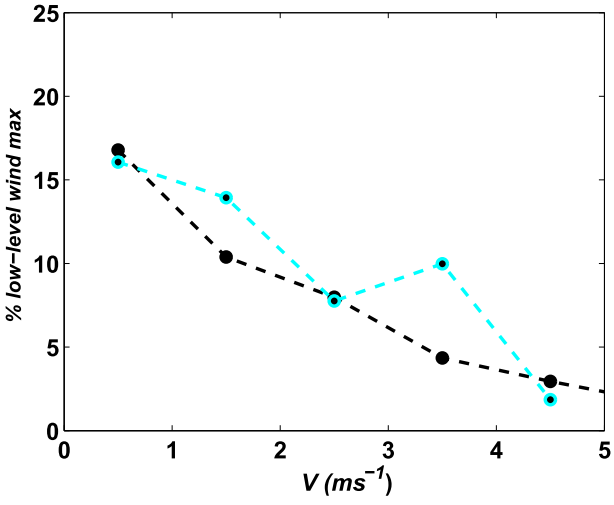

FIG. 8. The percentage of occurrence of near-surface wind maxima below 5 m for the entire field program for $R_{net} < -50\,W\,m^{-2}$, as a function of the speed of the along-valley wind component at 20 m (black) and the speed of the cross-valley component at 20 m (cyan).

most studies in the literature, the downvalley flow shows characteristics similar to larger valleys except that it is thinner and more vulnerable to elimination by modest increases of the regional wind speed. The downvalley cold air drainage is typically about 5-m deep with a maximum speed at 1 m of about $0.5\,m\,s^{-1}$. Surface-layer similarity theory is invalid for these cases (section 4). Cold air drainage down the valley generally forms with mostly clear skies and wind speeds less than $2\,m\,s^{-1}$ at the 20-m level (about 8 m above the valley top). However, the relation of the downvalley drainage of cold air to the ambient wind, stratification, and cloud cover is complex and a study in itself.

A case study assessment of the momentum budget indicates that the buoyancy generation of downvalley drainage flow exceeds the stress divergence corresponding to a net acceleration that is comparable to the observed acceleration ($d\bar{u}/dt$). The baroclinic term (thermal wind) due to modest decrease of the air temperature in the downvalley direction opposes the drainage flow but appears to be of marginal importance as found in previous studies. Other contributions to the along-slope pressure gradient are more difficult to evaluate but appear to be unimportant.

The near-surface wind maxima are generally transient and eliminated by modest variations of the regional wind field through increased vertical mixing. Computation of the turbulence profile for such conditions required reduction of the influence of nonturbulent motions on the calculated velocity fluctuations. We have used the turbulent velocity scale $V_{w\theta}$ (section 2), which is less vulnerable to the influence of nonturbulent motions compared to σ_w or the kinetic energy of the fluctuations. The turbulence reaches a local minimum at the wind maximum and is considerably stronger above the cold air drainage. This stronger turbulence may be part of a regional boundary layer above the numerous shallow valleys. The response of the vertical structure of the turbulence to the near-surface wind maximum implies that the turbulence is primarily finescale during periods of downvalley drainage flow and only weakly coupled to the overlying more significant turbulence. A future study will concentrate on the elimination of the downvalley cold air drainage through transient increases of the regional flow and vertical mixing.

Acknowledgments. We gratefully acknowledge the very helpful comments of Robert Heald, Branko Grisogono, and three reviewers. This work was supported by the National Science Foundation through Grant AGS-1115011. The SCP data were provided by the Integrated Surface Flux System of the Earth Observing Laboratory of the National Center for Atmospheric Research. The Earth Observing Laboratory is particularly acknowledged for rapid replacement and exhaustive system rechecking at the beginning of the experiment when extensive instrumentation damage occurred as a result of lightning. Any opinions, findings and conclusions or recommendations expressed in this publication are those of the author(s) and do not necessarily reflect the views of the National Science Foundation.

REFERENCES

Amanatidis, G., K. Papadopoulos, J. Bartzis, and C. Helmis, 1992: Evidence of katabatic flows deduced from a 84 m meteorological tower in Athens, Greece. *Bound.-Layer Meteor.,* **58,** 117–132, doi:10.1007/BF00120754.

Aubinet, M., B. Heinesch, and M. Yernaux, 2003: Horizontal and vertical CO_2 advection in a sloping forest. *Bound.-Layer Meteor.,* **108,** 397–417, doi:10.1023/A:1024168428135.

Blumen, W., 1984: An observational study of instability and turbulence in nighttime drainage winds. *Bound.-Layer Meteor.,* **28,** 245–269, doi:10.1007/BF00121307.

Caughey, S., and S. Palmer, 1979: Some aspects of turbulence structure through the depth of the convective boundary layer. *Quart. J. Roy. Meteor. Soc.,* **105,** 811–827, doi:10.1002/qj.49710544606.

Conangla, L., and J. Cuxart, 2006: On the turbulence in the upper part of the low-level jet: An experimental and numerical study. *Bound.-Layer Meteor.,* **118,** 379–400, doi:10.1007/s10546-005-0608-y.

Costa, F. D., O. C. Acevedo, J. C. M. Mombach, and G. A. Degrazia, 2011: A simplified model for intermittent turbulence in the nocturnal boundary layer. *J. Atmos. Sci.,* **68,** 1714–1729, doi:10.1175/2011JAS3655.1.

Coulter, R., and T. Martin, 1991: A comparison of nocturnal drainage flow in three tributaries. *J. Appl. Meteor.,* **30,** 157–169, doi:10.1175/1520-0450(1991)030<0157:ACONDF>2.0.CO;2.

——, and ——, 1996: Effects of stability on the profiles of vertical velocity and its variance in katabatic flow. *Bound.-Layer Meteor.,* **81,** 23–33, doi:10.1007/BF00119397.

Doran, J. C., and T. W. Horst, 1981: Velocity and temperature oscillations in drainage winds. *J. Appl. Meteor.,* **20,** 361–364, doi:10.1175/1520-0450(1981)020<0361:VATOID>2.0.CO;2.

——, ——, and C. D. Whiteman, 1990: The development and structure of nocturnal slope winds in a simple valley. *Bound.-Layer Meteor.,* **52,** 41–68, doi:10.1007/BF00123177.

Grisogono, B., and J. Oerlemans, 2001: Katabatic flow: Analytical solution for slowly varying eddy diffusivities. *J. Atmos. Sci.,* **58,** 3349–3354, doi:10.1175/1520-0469(2001)058<3349:KFASFG>2.0.CO;2.

——, L. Kraljević, and J. Jeričević, 2007: The low-level katabatic jet height versus Monin–Obukhov height. *Quart. J. Roy. Meteor. Soc.,* **133,** 2133–2136, doi:10.1002/qj.190.

Gryning, S.-E., L. Mahrt, and S. Larsen, 1985: Oscillating nocturnal slope flow in a coastal valley. *Tellus,* **37A,** 196–203, doi:10.1111/j.1600-0870.1985.tb00281.x.

Haiden, T., and C. Whiteman, 2005: Katabatic flow mechanisms on a low-angle slope. *J. Appl. Meteor.,* **44,** 113–126, doi:10.1175/JAM-2182.1.

Helmis, C., 1996: Some aspects of the variation with time of katabatic flow over a simple slope. *Quart. J. Roy. Meteor. Soc.,* **122,** 595–610, doi:10.1002/qj.49712253103.

Horst, T. W., and J. C. Doran, 1986: Nocturnal drainage flows on simple slopes. *Bound.-Layer Meteor.,* **34,** 263–286, doi:10.1007/BF00122382.

——, and ——, 1988: The turbulence structure of nocturnal slope flow. *J. Atmos. Sci.,* **45,** 605–616, doi:10.1175/1520-0469(1988)045<0605:TTSONS>2.0.CO;2.

——, and S. P. Oncley, 2006: Corrections to inertial-range power spectra measured by CSAT3 and Solent sonic anemometers, 1. Path-averaging errors. *Bound.-Layer Meteor.,* **119,** 375–395, doi:10.1007/s10546-005-9015-7.

Mahrt, L., 1982: Momentum balance of gravity flows. *J. Atmos. Sci.,* **39,** 2701–2711, doi:10.1175/1520-0469(1982)039<2701:MBOGF>2.0.CO;2.

——, 2010: Variability and maintenance of turbulence in the very stable boundary layer. *Bound.-Layer Meteor.,* **135,** 1–18, doi:10.1007/s10546-009-9463-6.

——, 2011: The near-calm stable boundary layer. *Bound.-Layer Meteor.,* **140,** 343–360, doi:10.1007/s10546-011-9616-2.

——, J. C. André, and R. Heald, 1982: On the depth of the nocturnal boundary layer. *J. Appl. Meteor.,* **21,** 90–92, doi:10.1175/1520-0450(1982)021<0090:OTDOTN>2.0.CO;2.

——, D. Vickers, R. Nakamura, J. Sun, S. Burns, D. Lenschow, and M. Soler, 2001: Shallow drainage and gully flows. *Bound.-Layer Meteor.,* **101,** 243–260, doi:10.1023/A:1019273314378.

——, C. Thomas, S. Richardson, N. Seaman, D. Stauffer, and M. Zeeman, 2013: Non-stationary generation of weak turbulence for very stable and weak-wind conditions. *Bound.-Layer Meteor.,* **147,** 179–199, doi:10.1007/s10546-012-9782-x.

Manins, P. C., 1992: Vertical fluxes in katabatic flows. *Bound.-Layer Meteor.,* **60,** 169–178, doi:10.1007/BF00122066.

McNider, R. T., 1982: A note on velocity fluctuations in drainage flows. *J. Atmos. Sci.,* **39,** 1658–1660, doi:10.1175/1520-0469(1982)039<1658:ANOVFI>2.0.CO;2.

Monti, P. F., W. Chan, M. Princevac, T. Kowalewski, and E. Pardyjak, 2002: Observations of flow and turbulence in the nocturnal boundary layer over a slope. *J. Atmos. Sci.,* **59,** 2513–2534, doi:10.1175/1520-0469(2002)059<2513:OOFATI>2.0.CO;2.

Mori, M., and T. Kobayashi, 1996: Dynamic interaction between observed nocturnal drainage winds and a cold air lake. *J. Meteor. Soc. Japan,* **74,** 247–258.

Nadeau, D. F., E. R. Pardyjak, C. W. Higgins, H. Huvald, and M. B. Parlange, 2013: Flow during the evening transition over steep alpine slopes. *Quart. J. Roy. Meteor. Soc.,* **139,** 607–624, doi:10.1002/qj.1985.

Oerlemans, J., and B. Grisogono, 2002: Glacier winds and parameterisation of the related surface heat fluxes. *Tellus,* **54,** 440–452, doi:10.1034/j.1600-0870.2002.201398.x.

——, H. Bjørnsson, F. Kuhn, F. Obleitner, F. Palsson, C. Smeets, H. Vugts, and J. D. Wolde, 1999: Glacio-meteorological investigation on Vatnajøkull, Iceland, summer 1996: An overview. *Bound.-Layer Meteor.,* **92,** 3–26, doi:10.1023/A:1001856114941.

Papadopoulos, K., C. Helmis, A. T. Soilemes, J. Kalgiros, P. G. Papageorgas, and D. N. Asimakopoulos, 1997: The structure of katabatic flows along a simple slope. *Quart. J. Roy. Meteor. Soc.,* **123,** 1581–1601, doi:10.1002/qj.49712354207.

Parmhed, O., J. Oerlemans, and B. Grisogono, 2004: Describing surface fluxes in katabatic flow on Breidamerkurjøkull, Iceland. *Quart. J. Roy. Meteor. Soc.,* **130,** 1137–1151, doi:10.1256/qj.03.52.

Porch, W., W. Clements, and R. Coulter, 1991: Nighttime valley waves. *J. Appl. Meteor.,* **30,** 145–156, doi:10.1175/1520-0450(1991)030<0145:NVW>2.0.CO;2.

Poulos, G. S., J. E. Bossert, T. B. McKee, and R. A. Pielke Sr, 2007: The interaction of katabatic flow and mountain waves. Part II: Case study analysis and conceptual model. *J. Atmos. Sci.,* **64,** 1857–1879, doi:10.1175/JAS3926.1.

Schmidli, J., and R. Rotunno, 2012: Influence of the valley surroundings on valley wind dynamics. *J. Atmos. Sci.,* **69,** 561–577, doi:10.1175/JAS-D-11-0129.1.

Smeets, C. J. P. P., P. G. Duynkerke, and H. F. Vugts, 1998: Turbulence characteristics of the stable boundary layer over a mid-latitude glacier. Part I: A combination of katabatic and large-scale forcing conditions. *Bound.-Layer Meteor.,* **87,** 117–145, doi:10.1023/A:1000860406093.

Stone, G., and D. Hoard, 1989: Low-frequency velocity and temperature fluctuations in katabatic valley flows. *J. Appl. Meteor.,* **28,** 477–488, doi:10.1175/1520-0450(1989)028<0477:LFVATF>2.0.CO;2.

Sun, J., 2007: Tilt corrections over complex terrain and their implication for CO_2 transport. *Bound.-Layer Meteor.,* **124,** 143–159, doi:10.1007/s10546-007-9186-5.

——, and Coauthors, 2004: Atmospheric disturbances that generate intermittent turbulence in nocturnal boundary layers. *Bound.-Layer Meteor.,* **110,** 255–279, doi:10.1023/A:1026097926169.

——, D. Lenschow, L. Mahrt, and C. Nappo, 2013: The relationships among wind, horizontal pressure gradient, and turbulent momentum transport during CASES-99. *J. Atmos. Sci.,* **70,** 3397–3414, doi:10.1175/JAS-D-12-0233.1.

Thomas, C., A. Kennedy, J. Selker, A. Moretti, M. Schroth, A. Smoot, and N. Tufillaro, 2012: High-resolution fibre-optic temperature sensing: A new tool to study the two-dimensional structure of atmospheric surface-layer flow. *Bound.-Layer Meteor.,* **142,** 177–192, doi:10.1007/s10546-011-9672-7.

van der Avoird, E., and P. Duynkerke, 1999: Turbulence in katabatic flow. Does it resemble turbulence in stable boundary layers over flat surfaces? *Bound.-Layer Meteor.,* **92,** 37–66, doi:10.1023/A:1001744822857.

Whiteman, C., 2000: *Mountain Meteorology*. Oxford University Press, 355 pp.

Williams, A., S. Chambers, and S. Griffiths, 2013: Bulk mixing and decoupling of the stable nocturnal boundary layer characterized using a ubiquitous natural tracer. *Bound.-Layer Meteor.,* **149,** 381–402, doi:10.1007/s10546-013-9849-3.